Colloids and Surfaces A: Physicochemical and Engineering Aspects 652 (2022) 129825

Contents lists available at ScienceDirect

Colloids and Surfaces A: Physicochemical and Engineering Aspects

journal homepage: www.elsevier.com/locate/colsurfa

Dual functionality of ultralow levels of a model kinetic hydrate inhibitor on hydrate particle morphology and interparticle force

Joshua E. Worley [1], Jose G. Delgado-Linares [2], Carolyn A. Koh [*,3]

Department of Chemical and Biological Engineering, Center for Hydrate Research, Colorado School of Mines, Golden, Colorado 80401, United States

HIGHLIGHTS

- Interparticle hydrate forces at short contact times are reduced by 40–54 % with ultralow levels of PVP (ul-PVP).
- Sintering forces at contact times up to an hour are decreased by 20–40 % with ul-PVP.
- Hydrate film growth rates are retarded by 30–50 % and long and short-term morphology changes are induced with ul-PVP.
- Nucleation and growth inhibition begins at concentrations as low as 0.01 wt% PVP.

GRAPHICAL ABSTRACT

Key effects of low concentration polyvinylpyrrolidone (PVP) on cyclopentane hydrates.

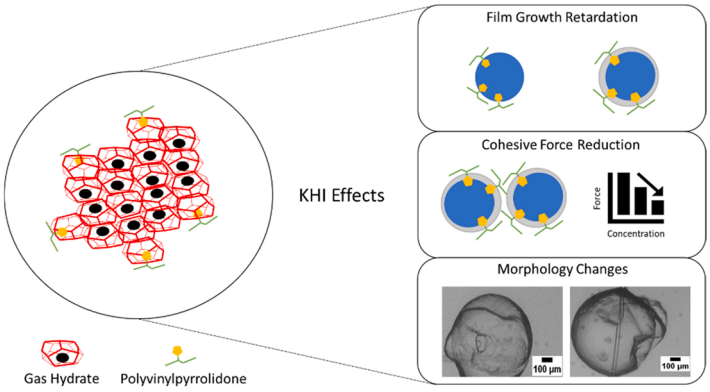

ARTICLE INFO

Keywords:
Interface
Adsorption
Kinetic inhibition
Hydrate morphology
Interparticle force
Gas hydrates

ABSTRACT

Gas hydrate plug formation is a major concern in oil and gas exploitation efforts, wherein line blockages can pose major safety, economic, and environmental risks. Kinetic hydrate inhibitors (KHIs) are a promising class of hydrate management chemicals, which are potentially cleaner, cheaper, and greener than traditional thermodynamic hydrate inhibitors (THIs). Therefore, understanding the effects that KHIs have on hydrate particles is vital to their application. In this study, polyvinylpyrrolidone (PVP), a model KHI, was investigated at ultralow concentrations to determine its effect on the properties of hydrates and elucidate when nucleation and growth inhibition begins. It was found that PVP can adsorb at the hydrate particle surface to reduce interparticle force by 40–54 %. Low concentration PVP continues to affect interparticle forces at prolonged contact times, reducing forces at 30-minutes to 1-hour of contact by 20–40 % and reducing sintering rate. PVP also reduces film growth rates by 30–50 % depending on the concentration of PVP in the water phase. The onset of major nucleation and growth effects was observed to occur at 0.01 wt% PVP in the water phase, two orders of magnitude below concentrations typically employed in hydrate management. It was discovered that low dosage PVP can cause

Abbreviations: KHI –, Kinetic hydrate inhibitor; AA –, Anti agglomerant; THI –, Thermodynamic hydrate inhibitor; AFP –, Antifreeze protein.

* Corresponding author.
E-mail address: ckoh@mines.edu (C.A. Koh).
[1] ORCiD https://orcid.org/ 0000-0003-0706-9716
[2] ORCiD https:// orcid.org/0000-0001-9266-1225
[3] ORCiD https://orcid.org/0000-0003-3452-4032

https://doi.org/10.1016/j.colsurfa.2022.129825
Received 7 June 2022; Received in revised form 25 July 2022; Accepted 28 July 2022
Available online 29 July 2022

major morphological changes to the hydrate particles in both the short and long term, which can influence interparticle forces and particle agglomeration, and may serve as a morphological screening tool for KHIs. A proposed mechanism for the observed morphology changes explains how the heterogenous adsorption of chemicals at the particle surface can lead directly to the newly observed particle morphology. The results presented in this paper show that ultralow concentrations of KHIs (0.0005 wt%) can have combined effects on the interfacial activity and crystal growth and morphology of hydrates, showing KHIs to be a dual function inhibitor of both interparticle interactions and hydrate growth. These results can inform KHI applications from industrial flow assurance to carbon dioxide transport for unimpeded carbon capture and sequestration.

1. Introduction

Gas hydrates are clathrate inclusion compounds generally formed at high pressures and low temperatures when small guest molecules (such as methane and carbon dioxide) are surrounded by stabilized water cages [1]. These compounds hold promise as vessels for carbon sequestration, clean hydrogen transport, and future clean energy sources in the form of natural deposits of methane hydrate [2–6]. However, gas hydrates also pose major economic, safety, and environmental concerns to current energy supplies. They are often encountered in the oil and gas industry, specifically in undersea oil and gas exploration, where prime conditions for hydrate formation are often encountered [7,8]. The prevention and control of hydrates in subsea pipelines has thus become a major area of research in the energy industry.

THIs are traditionally employed to shift the pipeline fluids out of the hydrate stability region. This often requires large volumes (e.g., 40 % or more) of chemical additives, such as methanol or glycol, which increases both environmental concerns and operating costs, as well as making downstream separations more difficult and expensive. Further, as reservoir conditions change, so does the required volume of THIs, hence total hydrate inhibition is not viable as a preventative measure.[9,10] Thus, research has shifted to focus on hydrate management, rather than hydrate prevention [7,11]. In hydrate management schemes, hydrate particles are allowed to form, but low dosage additives are added to either lower interparticle forces (anti-agglomerants, AAs) or slow the formation of the hydrate particles (kinetic hydrate inhibitors, KHIs), such that the time to formation is longer than the residence time of the fluid in the hydrate forming region [12]. These low dosage inhibitors generally target different steps during the formation of hydrate blockages, the overall process of which is depicted in Fig. 1, with the areas which KHIs target highlighted. AAs target the agglomeration step, while KHIs target the induction and film growth steps.

AAs are surfactants which adsorb onto the surface of the hydrate particles and reduce the cohesion forces. They allow hydrates to form, but keep the particles small and dispersed in the bulk phase, forming a transportable slurry [15]. AAs are often required in very small volume, (generally 2–3 wt% but sometimes less than 0.5 wt%), and have been proven effective at reducing the interparticle cohesive forces, sometimes to unmeasurable levels, even at long contact times before the onset of sintering [16,17]. AAs work at both high and low subcooling and can remain effective at preventing plug formation even during shut-in periods [18]. However, AAs often fail at high water content (e.g., above ~50 vol%), and require that there be a bulk hydrocarbon phase to properly align themselves at the interface and prevent interparticle

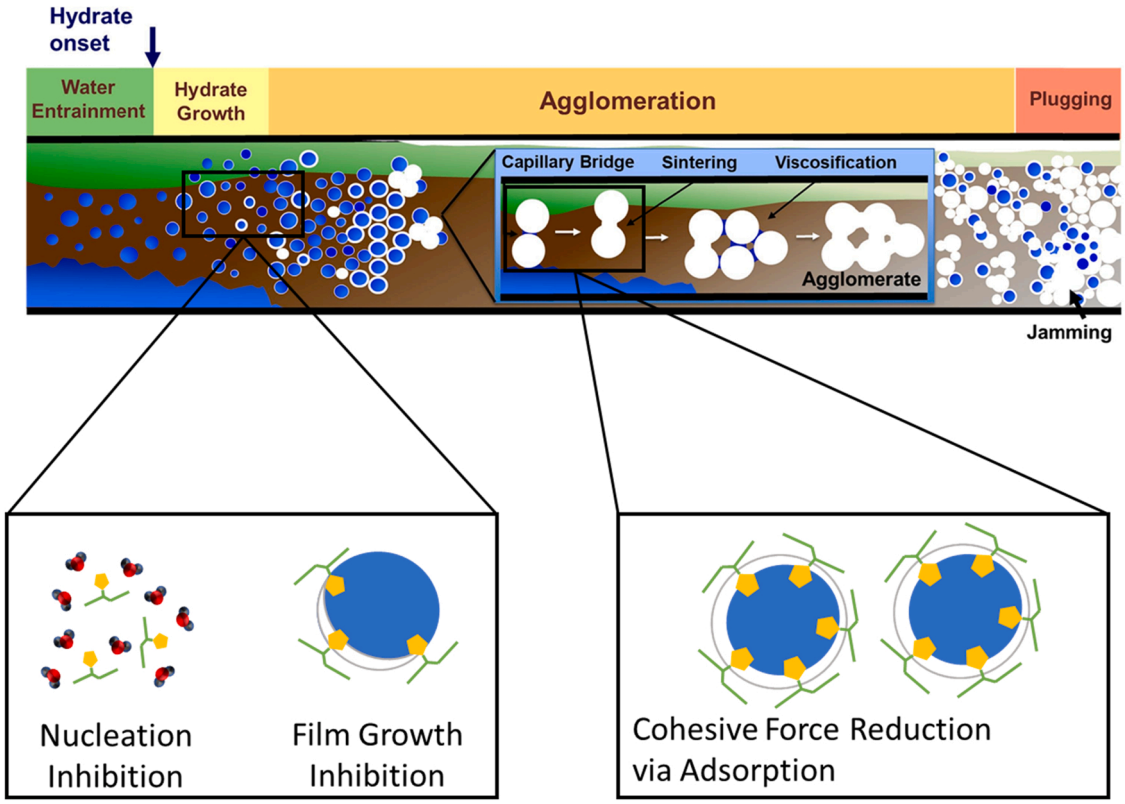

Fig. 1. Hydrate plug formation mechanisms in liquid hydrocarbon dominated systems with KHI targets highlighted. Green represents gas phase, brown represents the liquid hydrocarbon phase, blue represents the aqueous phase, and white represents gas hydrate.
Modified from Turner [13]; Stoner and Koh.[14].

interactions [19]. The water content limitation can be especially challenging in mature fields with higher water content, and in enhanced oil recovery applications. Further, the requirement of a liquid hydrocarbon phase makes AAs unusable in gas dominated systems.

KHIs are typically water-soluble polymers which extend the time required for hydrate shell formation and growth. It has been proposed that most KHIs operate through surface adsorption and steric hindrance during hydrate formation or through a perturbation-inhibition mechanism [20–22]. It is also possible that there is a combination of inhibition mechanisms contributing to the total inhibitory effect [23]. KHIs often struggle to prevent hydrate formation at the high subcoolings (>10 °C) encountered in deep sea pipelines, and their efficacy may diminish during shut-in conditions, which can extend beyond the induction time delay induced by the KHI. However, unlike AAs, KHIs can function in systems with high water content and in gas dominant systems, as they dissolve in the water phase [24]. KHIs target hydrate formation before the onset of major particle formation and may also introduce changes to the interface, which could affect interparticle interactions.

A study by Wu et al. [25] suggested that some KHIs may have anti-agglomerant properties. The addition of polyvinyl caprolactam (PVCap) was shown to reduce hydrate interparticle cohesive forces by 45–54% depending on dosing procedure. The reduction in force did not vary widely as a function of PVCap concentration (in the range of 0.005–0.5 wt%) or temperature at a contact time of 10 s. The time to total film coverage when contacting a hydrate particle and a water droplet containing PVCap at 0.5 wt% was significantly longer than pure water film growth at large subcooling [25]. Wu et al. also applied a dosing procedure for their PVCap experiments which involved a replacement of the bulk fluid surrounding the hydrate particles. However, due to problems with hydrate dissociation during the fluid replacement, the current study developed a new dosing procedure that avoided potential partial hydrate dissociation and uncertainty in KHI concentration by avoiding the replacement of the bulk solution the hydrate particles were placed in.

These previous results did not directly show that KHIs could serve dual purpose (AA and KHI) as hydrate management chemicals at extended contact times. Contact time plays a vital role in determining the mechanism of interparticle interactions, determining the cross over between capillary liquid bridge forces and sintering interactions [26]. AAs have been shown to be effective even at long contact times, but KHIs have not been studied for their effects on interparticle force at long contact times. Since KHIs reduce the film growth rate, it is reasonable to propose that they could slow the sintering behavior of hydrate particles, which would be important for shut in scenarios involving hydrates with surface adsorbed KHIs. Therefore, part of this study aimed to correlate the reduction in film growth rate with reduction in sintering force at contact times of up to an hour.

Many studies have shown that AAs have a pronounced effect on the hydrate morphology, and that this morphological change can be used as a screening tool for effective AAs [27–30]. Generally, the more morphological change that is experienced, the better the AA is suggested to function. However, these morphology effects have not been well documented for KHIs, except in limited single crystal and film growth studies [31–34]. The present study aims to show that even ultralow KHI dosages can cause drastic changes to hydrate particle morphology on both short and long timescales and give a conceptual understanding of why these morphological changes occur. This is important to document for KHIs, as changes in morphology can contribute to changes in the interparticle force and agglomeration behavior. This study further aims to show that the morphological changes, as well as the changes in interparticle force, can be explained by stochastic adsorption of PVP to the surface of the hydrate particle, with areas of high concentration showing drastic morphology changes and differing interaction behavior.

The morphology of hydrate particles can have an effect on particle interactions, and can be influenced by the addition of chemicals, such as surfactants, AA's, and KHIs [35,36]. Morphology changes are generally attributed to changes in the hydrate growth behavior, crystal morphology, mass and heat transfer characteristics, or the formation, interaction, and growth of hydrate crystals at water-hydrate former interfaces. In some cases, completely new morphologies are observed with just small changes in the system. Visualizing and documenting the morphology changes caused by single chemical additives (such as KHIs) is thus vital to understanding the totality of the effects of the additive on the hydrate forming system.

A large body of previous work has examined the effect of KHI concentration (generally in the range of 1–3 wt%) on hydrate nucleation and growth. However, no previous study has looked at ultralow concentrations of KHI where the induction delay may not be large, but macroscopic effects to morphology, film growth rate, and interparticle force can still be observed. Thus, this present study aims to investigate how concentrations of KHI less than 0.01 wt% can affect macroscopic quantities, like film growth rate, morphology, and interparticle force. Further, this study aims to provide a lower bound on the concentration at which a kinetic inhibitor begins to affect nucleation and growth of the hydrate particles.

This paper advances fundamental knowledge of the effects of ultralow levels of KHIs on hydrate particles. The results conferred will aid in the development of better, cheaper, and greener hydrate prevention strategies, which could be applied in flow assurance and could also be of major use in advancing carbon dioxide transportation for sequestration and hydrogen transportation for clean energy.

2. Materials and methods

2.1. Materials

Cyclopentane hydrates were formed utilizing 99.8 % pure cyclopentane (purchased from OmniSolv). Deionized water utilized in the experimentation and in making the KHI solutions was produced with a Millipore filtration system. The polyvinylpyrrolidone $(C_6H_9NO)_n$ used as the model KHI in the studies (purchased from VWR Life Sciences) has a purity of 99% and molecular weight of 40,000. All experiments were performed at a temperature of 1.2 degrees Celsius (ΔT_{sub} of 6.5 degrees Celsius).

2.2. Low pressure MMF apparatus

Hydrate cohesive forces were all measured utilizing an in-house Low-Pressure Micro Mechanical Force (MMF) apparatus, described in detail by Yang et al. and Taylor et al. [37,38]. A camera (resolution of 3.75 μm/pixel, 10 frames/second capture rate) and microscope were oriented above a 50 mL aluminum cell surrounded by a glycol-water cooling jacket. The cell was filled with cyclopentane which was cooled and monitored with a Type T thermocouple. The MMF apparatus is maintained in a dry box to remove moisture effects. The apparatus contains two cantilevers which hold the hydrate particles: a stationary cantilever with known spring constant and a precision manipulated cantilever, which can be brought into contact with the stationary one. Water droplets are placed on each cantilever and submerged in liquid nitrogen to form ice particles, which are placed into the cooled bulk cyclopentane. Once both cantilevers were in the cell, the temperature of the cyclopentane was slowly brought up to the experimental temperature, whereupon the ice particles melted, and hydrates formed. At the observed onset of hydrate formation, a timer was set for 30 min, during which the hydrate particles continued to grow - this is referred to as the annealing time and was held constant at 30 min for all tests performed.

2.3. Dosing procedures for PVP

Since PVP is not directly soluble in the oil phase, a controllable water dosing mechanism had to be developed. Wu et. al [25] dosed PVCap by creating aqueous solutions of PVCap at the experimental concentrations

and adding this mixture to cyclopentane to create a water saturated cyclopentane bulk which they formed their hydrate particles in. To avoid the potential influence of added water on force results coupled with the uncertainty of the concentration of the KHI at the interface and the difficulty associated with replacement of the cyclopentane bulk without dissociating the hydrate particles, a new method was developed for better experimental control. As such, in this study, PVP was directly dosed into the water phase at low enough concentrations to allow for hydrate particle formation from PVP solutions, bypassing issues with bulk replacement and allowing tighter control of experimental conditions.

Powdered PVP was first weighed out to create 50 mL of a 1 wt% stock solution. This PVP was slowly added to a 50 mL volumetric flask containing 30 mL of DI water, which was agitated to help partially dissolve the PVP. Then, DI water was added to the 50 mL mark, and the flask was further agitated until all of the PVP dissolved, and the solution was clear (~10–20 min). The PVP solutions utilized ranged in concentration from 0.0005 to 0.01 wt%, these were prepared by diluting the 1 wt% stock solution to reach the desired concentration. The concentrations selected were much lower than those traditionally used in hydrate mitigation and provided insight into the long-term behavior of KHI's adsorbed onto the surface of the gas hydrate particles. Fig. 2 provides an overview of the dosing and hydrate formation procedure.

2.4. Particle-particle force measurements

To measure the force between the newly formed hydrate particles, the movable cantilever was manipulated such that the particles were brought into contact for a specified contact time. In this study, contact times of 10 s were used for the baseline force measurements and contact times of 1–60 min were used for the sintering inhibition tests. A full explanation of the procedure for the pull off measurements and the determination of the cohesive force is given by Aman et. al.[26] For the short contact time measurements, 40 pull offs were performed per particle pair to obtain good statistics for the average cohesive force. For the long contact time sintering measurements, one pull-off per particle pair was generally performed, except for the 1-minute trials during which a maximum of 10 pull offs per particle pair were performed (to reduce the effects of extended annealing time on the final results). As such, multiple data sets had to be combined during the analysis of the sintering data in order to obtain adequate statistics/error estimates. Further, the 30 min and 1 h sintered particles would sometimes separate slightly off screen due to the very strong forces holding them together, so estimates of the total separation distance were made in these cases. A brief sensitivity analysis yielded that there was no major change in the calculated average force as a function of separation distance estimates in a 10–20 pixel (30–60 μm) range, giving confidence that the estimation procedure for these special cases was accurate. Interparticle forces are implied by the capillary bridge model to be functions of the contact angle and are normalized by the harmonic radius of the two particles to remove particle size dependency [39].

At the end of the pull off measurements, the video was analyzed using ImageJ [40].

2.5. Film growth rate measurements

To quantify the effects of KHI concentration on the film growth rate of cyclopentane hydrates, hydrate particles of differing concentration were brought into contact with a liquid water phase containing different concentrations of PVP. Hydrate particles were formed with and without PVP to allow comparison of film growth rate and morphology as a function of surface adsorbed KHI concentration. After the hydrate particles were formed, small droplets of water with and without PVP were carefully placed on the hydrate surface and allowed to grow hydrate films. ImageJ [40] was used to track the advancing film front over varying time intervals, and an average growth rate was calculated for each droplet. The entire procedure was repeated for a minimum of 20 growth rate measurements for each case. The film growth measurement process is illustrated in Fig. 3.

Hydrate film growth rates are assumed to be functions of heat and mass transfer resistances [41–44] with very weak dependence on particle/interfacial area or film thickness (which are both hard to determine exactly from videos). As such, film growth rates are not normalized by area in line with other literature [45–48].

2.6. Particle morphology studies

The changes in morphology of the hydrate particles induced by the presence of PVP were studied throughout the experiments. Two separate morphological phenomena were observed. The first included morphological changes observed during the particle annealing process, termed initial growth morphology effects. The second type of morphological effects were gradual changes observed in the particle morphologies during 45-minute to 2-hour observation periods. These were referred to as long-term morphology effects/long-term shell effects. Videos and still images of both morphological phenomena were captured and sped up utilizing ImageJ [40] and online editing software.

3. Results and discussion

3.1. Baseline Cohesive Force

Baseline cohesive force measurements for 10 s contact times were performed with and without the presence of PVP and compared to the force documented by Aman et al. [26] Fig. 4 represents the average force across five experiments with 40 pull offs each for particles with 0, 0.0005, and 0.001 wt% PVP in the water phase. The error bars represent combined 95% confidence intervals calculated from the combined standard deviation and number of trials across the five experiments per particle pair.

Pure cyclopentane hydrate particles were prepared and tested first. The measurements produced a baseline cohesive force of 4.5mN/m

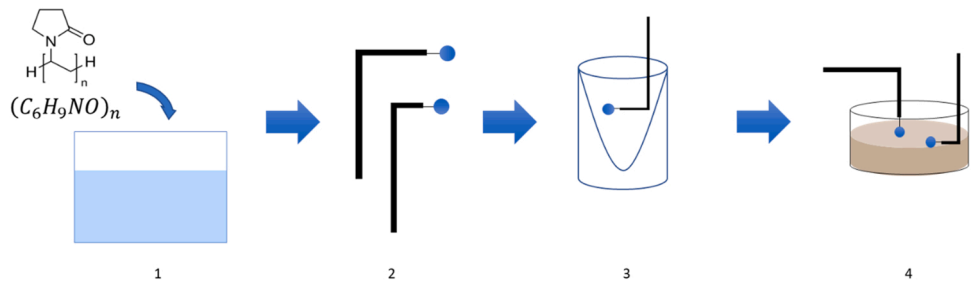

Fig. 2. PVP dosing method developed in this study. 1. Mix PVP in water at desired concentration and stir until completely dissolved. 2. Sample water and form droplets on cantilevers. 3. Fully submerge water droplets in liquid nitrogen to form ice. 4. Place cantilevers in cooled cyclopentane and slowly increase temperature to experimental temperature, allowing hydrates to form.

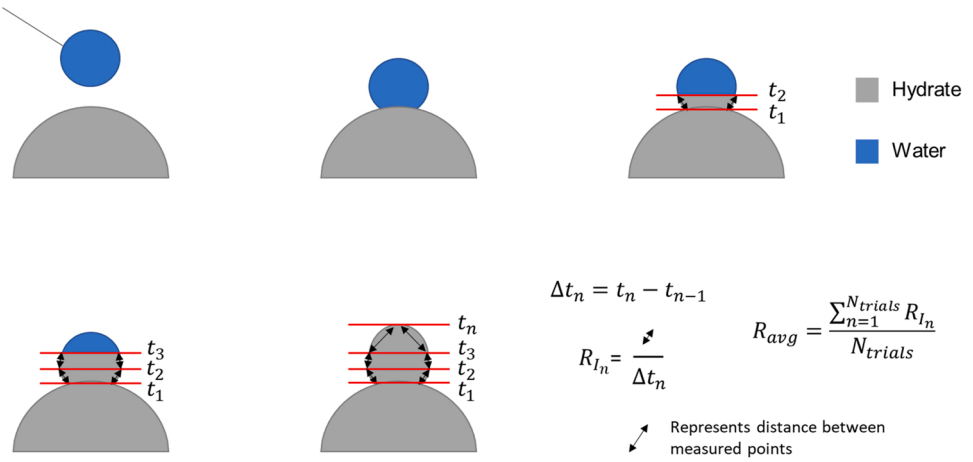

Fig. 3. Procedure for measurement of average film growth rate displaying measured quantities and equations used.

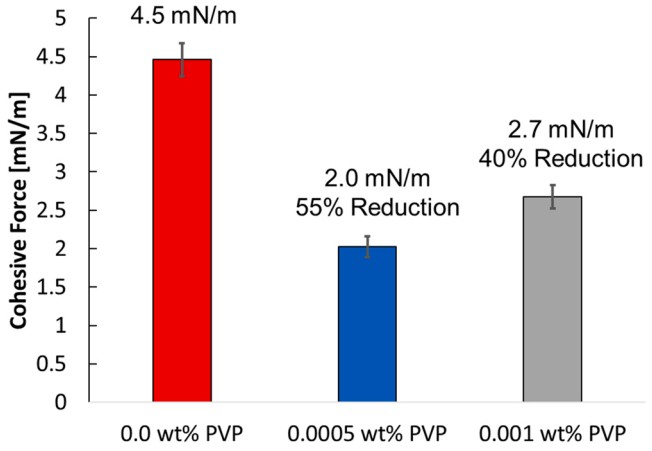

Fig. 4. Average cohesive force for 10 s contact time at two PVP concentrations on the hydrate surface compared to baseline pure hydrates. Error bars represent 95% confidence intervals over 3–5 sets of 30–40 trials for each concentration. Average force for each concentration: 0 wt% PVP 4.46 ± 0.22, 0.0005 wt% PVP 2.03 ± 0.13, 0.001 wt% PVP 2.65 ± 0.15. The percentage reductions in force are 54.6 ± 0.8 % for 0.0005 wt% PVP and 40.6 ± 0.5 wt% for 0.001 wt% PVP.

which matches the 4.2mN/m baseline presented by Aman et al. [26] Next, measurements were repeated with the addition of PVP. Only the two lowest concentrations, 0.0005 and 0.001 wt% PVP, were utilized due to the difficulty of forming hydrates when the PVP concentration was 0.01 wt% or above. The 10 s baseline force measurements, provided in Fig. 4, produced cohesive force values of 2.0 and 2.7 mN/m for the 0.0005 and 0.001 wt% PVP hydrates, respectively. These forces are 40–54 % lower than the pure cyclopentane baseline and seemed to be concentration independent, with both PVP systems experiencing similar decreases in force, which is consistent with previous studies [25]. Intuitively, the 0.001 wt% PVP particles should have lower forces than the particles with lower concentration since more polymer will be adsorbed at the interface. However, a combination of increased porosity, slower water conversion, and stochastic adsorption could explain why this is not the case. Most likely, there is more water at the surface of the hydrate particle of higher PVP concentration since, in the same annealing time, the particle containing the higher concentration of PVP would not have experienced water conversion as rapidly. Further, potentially increased shell porosity could allow more water to escape from the interior of the particle and form a layer at the surface, which would add to the liquid available for capillary bridge formation. As interparticle force is a strong function of the free water on the surface, these two mechanisms would serve to increase the force experienced at the higher concentration of PVP. Stochastic PVP adsorption could also play a small part in increasing the force seen at the higher concentration. Due to the random adsorption of the polymer on the hydrate surface, some areas could have little or no exposed PVP, and would act more like hydrate particles formed with 0 wt% PVP, which could increase the force experienced.

3.2. Film growth

Film growth experiments were performed by placing droplets of water with and without PVP onto the surface of pre-formed gas hydrate particles of varying concentrations to determine the effect of both the adsorbed PVP concentration (on the hydrate surface) and the concentration of PVP in the water on the film growth rate. The hydrate particles were formed with the standard procedure, and droplets of pure DI water and water with three concentrations of PVP were placed on the surface of the particles and monitored for 30 min to an hour. The film growth rate was then measured, and the results are presented in Fig. 5 with 95%

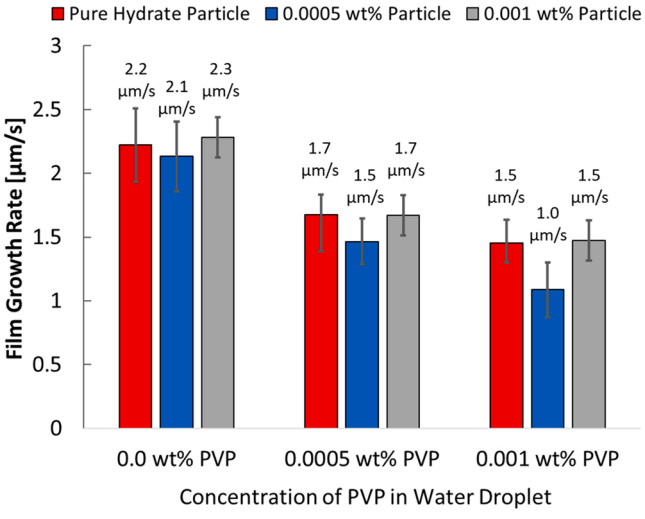

Fig. 5. Film growth rate of water droplets of varying PVP concentration placed on pure hydrate particles (red), and particles formed with 0.0005 wt% PVP (blue) and 0.001 wt% PVP (gray). Error bars represent 95 % confidence intervals of 20–30 measurements across 2–3 film growth trials for each hydrate particle. The overall decrease in film growth rate from 0 wt% PVP in the water droplet to 0.001 wt% PVP in the water droplet was 34.4 ± 2.0% for the pure hydrate particles, 55.2 ± 1.4 % for the 0.0005 wt% hydrate particles, and 35.5 ± 1.5% for the 0.001 wt% hydrate particles.

confidence intervals.

Only the two lower concentrations of PVP were utilized, since nucleation inhibition caused by the 0.01 wt% PVP made film growth measurements impossible (mostly) in a reasonable timeframe (~2 h). At the 0.0005 and 0.001 wt% concentrations, there was no major visual delay in the initial hydrate nucleation/film formation indicating a failure to function as induction inhibitors at such low concentrations. Three sets of film growth experiments were performed with particles formed with 0, 0.0005, and 0.001 wt% PVP and with water droplets of 0, 0.0005, and 0.01 wt% PVP. The concentration of PVP in which the hydrate particle was formed did not have significant effect on the film growth rate, but the concentration of PVP in the water droplets did have pronounced effect (Fig. 5). This is inferred from the similar average values for film growth rate for all three hydrate particle concentrations at each of the three aqueous concentrations (~2.2 μm/s for all three particles with pure DI water as the droplet, ~1.6 μm/s for all three particles with 0.0005 wt% PVP in the water droplet, and ~1.5 μm/s for all three particles with 0.001 wt% PVP in the water droplet). However, the film growth rate decreases significantly as the concentration of PVP in the water droplets increases for the three particle concentrations tested. For the pure hydrate particles, the film growth rate decreased 34% from the pure water droplet trial to the 0.001 wt% PVP water droplet trial. The 0.0005 wt% particles saw a 55 % decrease from the pure water case to the 0.001 wt% PVP water droplet case, and the 0.001 wt% particle experienced a 35% decrease in film growth rate from the pure water case to the 0.001 wt% PVP water case. Water spreading was not observed to occur during the course of the film growth measurements and even slight, unobservable water spreading would not be expected to greatly affect results or reproducibility [48].

Film growth rates are an important factor in hydrate management, as the formation of films on suspended water droplets and on water droplets in contact with pre-formed hydrate particles influences the rate at which hydrate particles and agglomerates can form and become strong/stable in the system. Slowing the film growth rates is thus a major impact of KHIs in flow assurance scenarios. This study suggests that perturbation inhibition, the ability of KHIs to inhibit hydrate nucleation by perturbing water structuring, may be a more effective film growth inhibition mechanism, since the aqueous concentration of PVP had greater effect on the film growth rate. This is an important observation for many reasons, but the largest is that, if designed correctly, lower dosages of KHIs can help manage hydrate formation risk, hence decreasing operating cost and environmental concerns associated with hydrate management.

3.3. Particle sintering

Sintering experiments were performed to examine the effect of PVP on interparticle force at long contact times which could be encountered in shut-in scenarios. The same procedure for the 10 s particle force measurements was followed for contact times ranging from 1 min to 1 h. Three concentrations of PVP, 0 wt%, 0.0005 wt%, and 0.001 wt%, were utilized, and their results given in Fig. 6 (representing the average sintering force for each concentration with error bars representing standard deviations calculated by combining data from all (5 or more) particle pair experiments for a particular concentration).

Since sintering depends on the growth of a film of hydrate across the liquid bridge between the hydrate particles, the film growth results suggest that the experiments where PVP is present in the system would have lower overall sintering forces due to slower and potentially weaker film formation. Further, the effects of the PVP on the hydrate shell, evidenced by the morphological changes documented, suggest that there should be effects on the sintering force.

On average, the particles with PVP exhibit lower sintering forces than the pure hydrate particles, a phenomenon that becomes more apparent as the contact time increases. At 1 min of contact, the pure hydrate particles exhibit an average force of 3.4 mN/m, while the

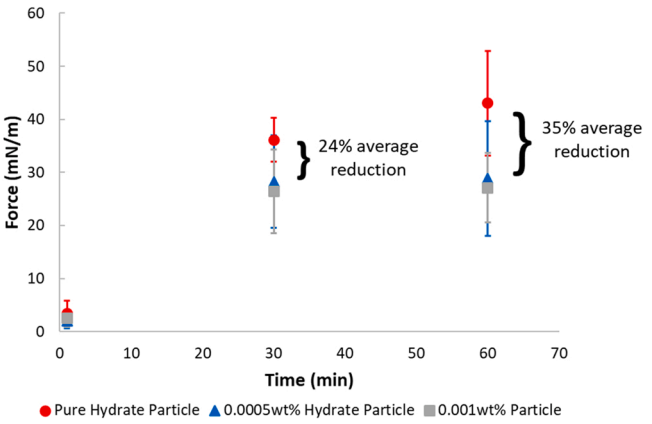

Fig. 6. Hydrate sintering force versus time for particles formed with 0 wt% PVP (red), 0.0005 wt% PVP (blue), and 0.001 wt% PVP (gray). Particles were annealed for 30 min and then put in contact for 1 min, 30 min, and 60 min to allow for sintering growth. Error bars represent standard deviations calculated by combining data across pull off measurements at each concentration. Since particles were all of similar size (diameters within 50–100 μm) effects of particle size on force is likely negligible. At least 5 experiments were conducted for each concentration at each annealing time. Measured sintering forces in mN/m are as follows: 1 min – 0 wt% PVP 3.40 ± 2.41, 0.0005 wt% PVP 1.98 ± 1.42, 0.001 wt% PVP 2.48 ± 1.58; 30 min- 0 wt% PVP 36.14 ± 4.17, 0.0005 wt% PVP 28.27 ± 8.69, 0.001 wt% PVP 26.43 ± 7.87; 60 min – 0 wt% PVP 43.03 ± 9.91, 0.0005 wt% PVP 28.79 ± 10.81, 0.001 wt% PVP 27.10 ± 6.54.

0.0005 and 0.001 wt% particles exhibit average forces of 2.0 and 2.5 mN/m respectively, representing 42 % and 27 % decreases from the pure hydrate case. At 30 min of contact, the forces start to deviate further. For the pure hydrate particles, the average force at 30 min of contact was 36.1 mN/m, while for the 0.0005 and 0.001 wt% particles, the average forces are 28.3 and 26.4 mN/m respectively, representing 22 % and 27% decreases. At 1 h of contact, the pure hydrate displayed an average force of 43.0 mN/m, while the 0.0005 and 0.001 wt% particles displayed average forces of 28.8 and 27.1 mN/m, representing 33% and 37% decreases, respectively. Though both concentrations of PVP performed similarly, the 0.001 wt% PVP starts to induce further force reductions as the contact time increases. It was also observed that, in some tests, the sintering force was too low to be measured (0/15 trials for 0 wt% PVP, 6/18 for 0.0005 wt% PVP, and 3/13 for 0.001 wt%PVP), while in others, the particles could not be separated or separated entirely outside of the observation window (3/15 trials for 0 wt% PVP, 3/18 for 0.0005 wt% PVP, and 2/13 for 0.001 wt% PVP). These phenomena indicate stochasticity in the behavior of the particles when PVP is adsorbed at the surface, but they could not be added to the average force and error determinations.

More information can be extracted from this data by looking at the increases in force across individual time steps. From the 1-minute experiment to the 30-minute experiment, all the sintering forces increased by between 11 and 14 times their measured 1-minute force. The reason for the similar initial sintering force increase is not fully understood, but it could be due to similar contributions to the force by the initial films that grow across the capillary bridge or interactions between the adsorbed PVP while it rearranges during initial film growth. However, from the 30-minute to the 60-minute experiments, the sintering force for the pure hydrate particles increased 19 % while the particles with PVP showed increases of only 1.8 % and 2.5 % for the 0.0005 and 0.001 wt% particles respectively. This data indicates that the PVP has a more visible impact on the interparticle interaction as contact time increases due to film growth rate reductions and potential film weakening as well as a potential change in the entropic or mass transfer resistances to growth caused by the PVP. PVP reduces the rate at which particles sinter by 15–17 % and reduces total sintering force by 22–37 %.

3.4. PVP effects on hydrate particle morphology

Changes in the macroscopic morphology of hydrate particles in the presence of AAs has been well documented and even proposed as a method for evaluating the efficacy of new AA chemicals or chemical mixtures.[28] KHIs have not been as widely studied for their morphological effects, especially at concentrations below those traditionally explored in hydrate research. As such, a major focus of this work was to document changes in particle-scale morphology with the addition of low-dosage PVP, and to provide theoretical explanation for the

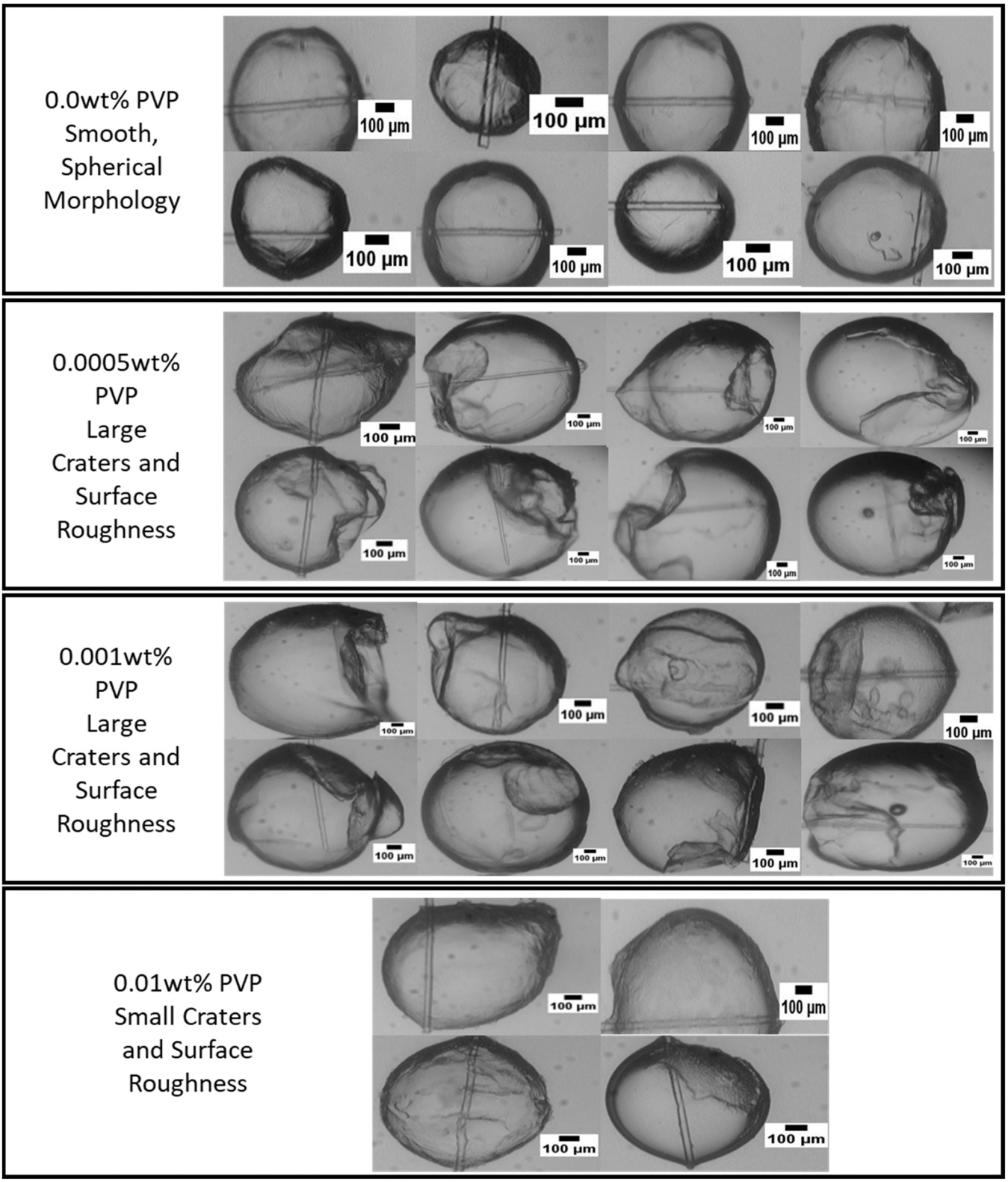

Fig. 7. Images of initial growth morphology at various concentrations taken during testing chosen to best illustrate the extent and diversity of morphological changes caused by surface adsorbed PVP.

morphology changes.

Images and videos were collected from several repeat experiments for all concentrations tested. During experimentation, it was noted that the morphology changes did not all occur at the same time. In some cases, the craters, or bumps on the surface of the particles were formed immediately or early on during the annealing period (Fig. 7). In other cases, the morphology of the particles continued to change throughout the course of the experiments, forming new craters or other new features all together. Such changes generally occurred from 45 min to two hours after the end of the particle annealing period and were referred to as long-term morphological/shell effects (Fig. 8).

For the initial growth morphology observations, morphologies were recorded immediately after the end of the annealing time. Fig. 7 provides images of the initial morphologies from separate experiments at all concentrations of PVP tested.

There are major morphological changes, namely increased roughness, and large craters, upon addition of PVP to the hydrate forming system, and the changes are similar across PVP concentrations. The rough morphology is also similar to some of the morphologies documented in water droplet growth experiments performed on structure I hydrates with antifreeze proteins (AFPs), [34,49] as well as planar hydrate film growth studies [33]. However, none of the previous work reported similar long-term morphological changes to those seen in this present work, and only Udegbunam et al. [49] observed crater formations similar to those seen here. Further, none of the polymeric KHIs previously tested display such major morphology changes that PVP has caused in this work. The lowest concentration of PVP mainly causes crater formation in the hydrate particles with little effect on the rest of the hydrate shell, apart from a few instances of increased surface roughness. For the intermediate concentration, many of the particles also experience this crater formation, and some of the particles become rough, with small pits and bumps in the hydrate film across the entire particle. At the highest concentration, film growth does not usually envelop the entire surface of the droplet, indicating film growth inhibition by PVP. However, the parts of the film that do form are rough like some of the intermediate and low concentration particles and show smaller scale craters like those seen in the other concentrations. Such morphology is not generally seen in the case of pure cyclopentane hydrates, meaning that morphology observations can allow for the detection of chemicals present in the system even at concentrations as low as 0.0005 wt% (5 ppm). It is further likely that more drastic changes to the particle morphology (or changes to the particle growth behavior) indicate higher concentrations of chemical were present, which would have direct effect on the hydrate properties including shell strength and interparticle force. The extent of morphology changes could potentially be used as a mechanism to rank the efficacy of the KHI.

To better quantify the observed initial morphological changes, all the videos for a particular concentration were examined, and the number of instances of morphological changes during the annealing period were recorded. These were then tabulated and are presented in Table 1. This analysis does not include particles which experienced long-term morphological changes to separate the morphological phenomena and prevent double counting of particles.

From Table 1, it is inferred that increasing the amount of PVP present increases the frequency with which particles experience morphology changes. Further, these morphology changes can be used to detect even trace amounts of kinetic inhibitors relatively easily.

Fig. 8 shows an image series extracted during long term observations of particles which demonstrate some of the long-term morphology changes that PVP can cause in the particles. The accompanying sped up videos of these phenomena are provided as videos S1-S4 in the

Table 1
Particle morphology changes. Determined by summing total number of particles of each concentration which experienced morphology changes and dividing by the total number of particles of each concentration formed during experimentation.

	Percentage of Particles Experiencing Morphology Changes Across Experiments		
	Total Number of Particles	Particles with Morphology Changes	Fraction of Particles with Morphology Changes
Pure Hydrate Particles	68	28	41 %
0.0005 wt% Particles	42	27	64 %
0.001 wt% Particles	43	34	79 %

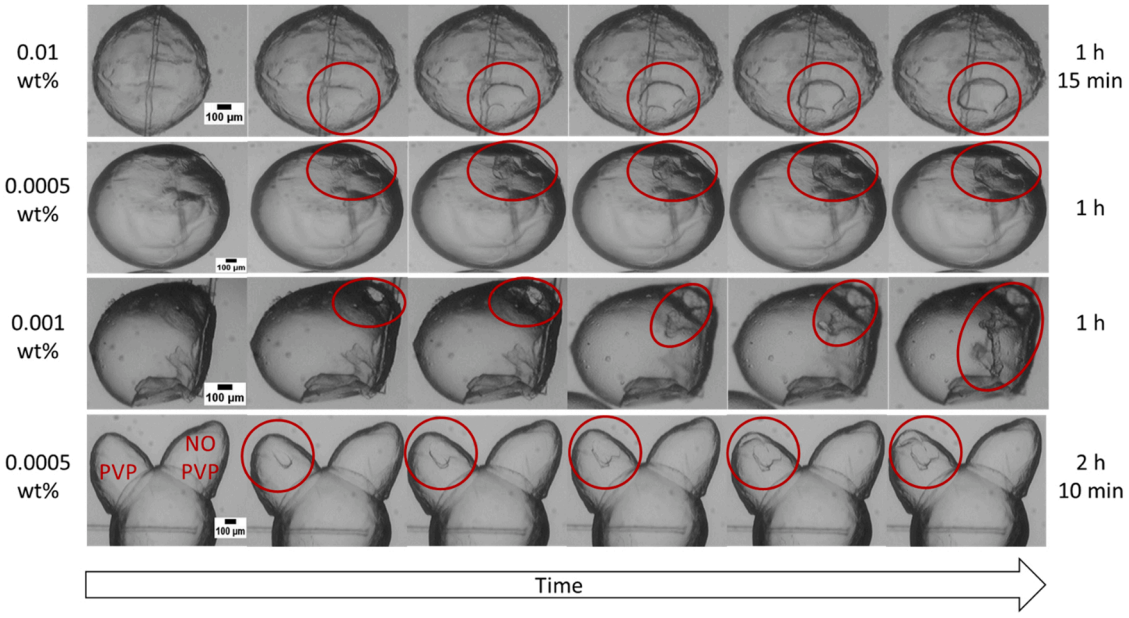

Fig. 8. Image series extracted over experimental duration for particles of varying concentration experiencing morphology changes separate from initial growth morphology. Times given are the times after the end of the annealing period over which morphology changes occurred. These images and the long-term changes to morphology indicate lasting impact of PVP on the shell properties.

supplementary materials.

Fig. 8 indicates that PVP induces prolonged effect on the hydrate shell and growth properties which could be important in field applications of KHIs. When PVP is present, the strength of the shell is inferred to be less than that of a pure cyclopentane hydrate, and the effect is long lasting. Further, when PVP is present, the shell is likely more porous, allowing water from the interior of the particle to escape. This has major implications for flow assurance, as the weaker shells could lead to easier hydrate breakup in turbulent lines, and the porosity of the shells could cause there to be larger water layers on the exterior of the particles.

Perhaps one of the more interesting observations of long-term morphological changes is that of the 0.0005 wt% film growth experiment (given as the final series in Fig. 8, and provided as video S4. Here, during film growth experiments, droplets of two different concentrations were placed on the particle surface and observed for two hours. The 'ear' on the left contained 0.0005 wt% PVP while the 'ear' on the right was DI water. Over the course of the observation, the droplet that contained PVP experienced a collapse/cave-in consistent with the observed changes in initial morphology for other particles, while the DI water droplet experienced no change to the shell morphology. This provides direct visual evidence that the PVP present in the system has long term effects on the shell strength. It also provides evidence that the retardation of water to hydrate conversion could be prolonged with PVP present, since the pressure equalization required to cause such morphological changes only occurs as water from the interior of the particle escapes and causes pressure differences. This further indicates that the effects of KHIs are long lasting and extend beyond just the initial slowing of nucleation and film growth.

A conceptual mechanism behind the morphology changes seen in the particles was developed to aid in understanding KHI working mechanisms (Fig. 9).

It is known that kinetic inhibitors have effects on the thickness of the hydrate film which can directly impact the strength of the film [49–51]. The morphological changes that were observed can be explained by the presence of PVP. PVP adsorbs stochastically to the hydrate surface, with areas of higher and lower concentration. The areas of higher concentration may have higher porosity and lower mechanical strength since thickening growth is slowed by the PVP. Other areas of the hydrate shell with lower relative concentration of PVP would likely be more porous than pure hydrate shells but would not experience extreme growth inhibition. The increased porosity of the hydrate shell allows water on the interior of the particle (which is slow to convert to hydrate due to the KHI and mass transfer limitations) to diffuse out of the particle more easily, causing the interior pressure to decrease. Since the shell is weaker in some areas, this pressure decrease causes the hydrate shell to cave-in and form craters at the sites of higher adsorption to establish pressure equilibrium. These cave-ins can then propagate in surrounding areas where the shell is still affected by the kinetic inhibitor, forming larger craters on the hydrate surface. A similar phenomenon can also apply to hydrates formed with low concentrations of natural AAs at low subcoolings as seen in a small number of experiments performed by the Center for Hydrate Research. Similar crater formations have been noted on hydrates grown with low concentrations of AAs likely due to the growth of weaker hydrate shells at lower subcoolings influenced by the interfacial adsorption of the AA molecules.

There is strong evidence that PVP can adsorb to solid surfaces in such a way that relatively large areas can have non-homogenous concentration. Flemming et al. [52] utilized soft-contact AFM to analyze the adsorption of PVP (10–200 ppm) at the solid graphite-liquid water interface. Though not exactly the same as the conditions of adsorption in this study, the random arrangement of the PVP into island-like structures before surface deposition/adsorption is analogous to the arrangement of the PVP at the hydrate surface in the current work and gives clear evidence for the natural formation of areas of high and low concentration on the surface of the hydrate particle. PVP forms a patchy film across the solid surface, with island-like structures of high and low concentration arising from polymer globule formation in solution before surface adsorption (Fig. 10A). This is very similar to the adsorption of PVP in this work.

The same phenomenon can take place at the surface of hydrates formed in the presence of AFPs, as evidenced by Fig. 10B from Gordienko et al. [53] In this study, Gordienko et al. formed hydrates with luminescent tagged AFPs (~60–700 ppm) and imaged them under a blacklight to examine if the AFP had adsorbed on the surface of the hydrate. The images show that there are brighter and darker spots on the surface of the hydrate particles, indicating areas of higher and lower protein adsorption respectively, and demonstrating that the "concentration islands" are observable in hydrate forming systems as well.

Explanations for these differing adsorption patterns on the solid surfaces seem to hinge on two primary mechanisms: polymer self-interaction and differing attachment to the solid surface, though these are likely compounded by molecular weight and concentration effects, which are explored in other articles [54,55]. In the current study, mass/diffusion limitations caused by the low concentration of PVP

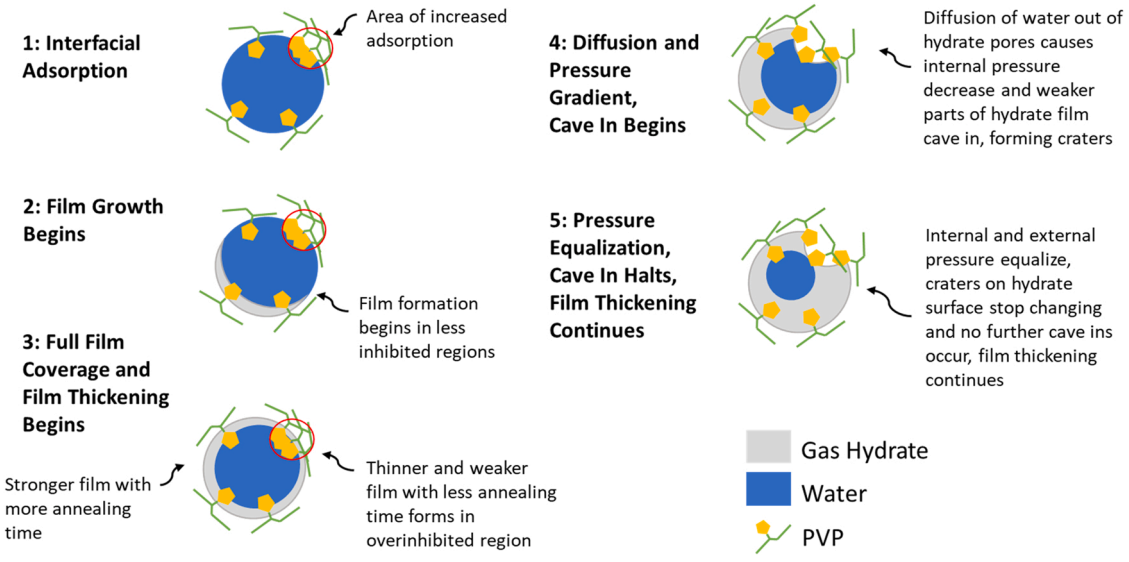

Fig. 9. Hypothesized mechanism for PVP induced morphological changes. Areas of increased concentration have weaker films which are prone to buckling, bulging, or caving-in/forming craters.

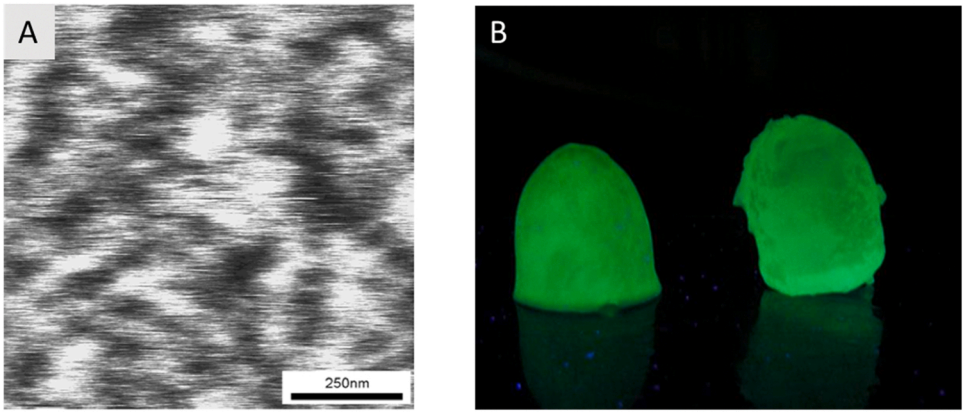

Fig. 10. A) Soft contact mode AFM images of PVP (200 ppm) adsorbed at a solid graphite surface displaying "islands" of localized concentration. High concentration areas are indicated by the white patches, while lower concentration areas are represented by the black patches. Though the concentrations utilized were higher than those in this study, localized islands of higher concentration can be seen by the very bright areas and localized areas of low concentration are seen by the darker splotches. It is expected that this effect is magnified for the lower concentration PVP utilized in this study.
(a) Utilized with permission from Flemming et al. [52] B) Surface distribution of fluorescently marked antifreeze proteins utilized as KHIs. (b) Utilized with permission from Gordienko et al. [53] copyright 2010 Gordienko et al. CCBY.

available to adsorb to the surface could magnify the effects of polymer aggregate formation seen in higher concentration systems.

3.5. Effects of higher PVP concentration

The 0.01 wt% particles are not included in Table 1, since inhibition (in several cases) of nucleation and growth made it difficult to sort these particles into those with simple morphology changes and those without. Fig. 7 shows four images of 0.01 wt% particles exhibiting full or partial film formation. These were rare exceptions for the 0.01 wt% particles. In the majority of cases, at 0.01 wt% PVP and above, nucleation inhibition or extremely low growth rates precluded the particles from growing strong enough films for testing in reasonable time frames. Therefore, separate morphological observations were made for the 0.01 wt% PVP trials. Videos S5-S7 presented in the supplementary materials show more commonly observed phenomena for this concentration, including sped up video clips of observations over 1 h or more displaying negligible film growth and nucleation. For a more in-depth look at the effects of the 0.01 wt% PVP on hydrate growth and morphology, a separate set of observations was tabulated and is presented in Table 2.

To better understand the effect of the 0.01 wt% PVP on the cyclopentane hydrates, a separate criterion was developed for this concentration and given in Table 2. In about 53% of the experiments performed with 0.01 wt% PVP, no nucleation or no significant film growth occurred. This was manifested in ice particles melting rather than serving as nucleation templates, lack of bulk nucleation on the water droplets, and lack of partial/complete film growth (even over 30 min to an hour of observation). In some cases, rather than growing a film when placed on the surface of a hydrate particle, the 0.01 wt% water droplets would begin to spread over the surface of the hydrate particle as seen in supplementary video S6 (2-hour observation). In about 27% of the 0.01 wt% experiments, the particles would form a partial film which exhibited very rough morphology and was craterous like the films at other concentrations of PVP. This is demonstrated in the bottom right image of the 0.01 wt% morphology images in Fig. 7. In only 20% of the experiments performed at 0.01 wt% PVP, a full film was formed over the surface of the water droplet. These films also exhibited the rough morphology seen at the lower concentrations. However, even after the 30-minute standard annealing time, these films were not strong enough to withstand even a single pull off as evidenced by video S7 in the supplementary material.

Table 2
Effects of 0.01 wt% PVP on hydrate particle formation detailing different phenomena observed during high concentration trials.

	Effect of 0.01 wt% PVP on Hydrate Morphology and Growth		
Total Number of Tests	Number of Particles with Full Film Growth	Number of Particles with Partial Film Growth	Number of Particles Exhibiting no Nucleation or Negligible Film Growth
15	3	4	8
Percentage of Total	20%	27%	53%

Upon close review, it seems that, even in cases of full film formation with 0.01 wt% PVP in the system, there may have been small areas over which a film had not formed which were obscured by the rough morphology. In contrast, the pure hydrates and the lower concentration PVP particles all formed complete shells of sufficient strength to withstand testing after half an hour of annealing. This is direct evidence for changes in the film properties (growth rate, porosity, shell strength/thickness) brought about by the PVP and is an important phenomenon to document for the application of KHIs. It is not only difficult to form a shell of hydrate in the presence of kinetic inhibitors of sufficient concentration, but the shell that does form is very weak, which could easily cause forming hydrates to break apart in turbulent flow. Further, if the particle film was destroyed, and the droplet surface was re-exposed, the time to hydrate formation would be extended, since a new film must grow over the exposed water surface.

The lack of film growth and nucleation at 0.01 wt% PVP is important to note for hydrate management applications. It suggests that the onset of kinetic inhibitory action relevant to flow assurance, namely nucleation and growth inhibition, in addition to decreased film strength over long timeframes, occurs at or around 0.01 wt% for PVP. This is useful in determining required dosages for applications of PVP to hydrate management.

4. Conclusion

A series of interfacial experiments were performed to determine the effects of PVP, a model kinetic hydrate inhibitor, on hydrate particles. The effect of the PVP on hydrate nucleation is negligible until a concentration of 0.01 wt%, which was found to be the onset concentration for nucleation and growth inhibition. For PVP concentrations of 0.0005 and 0.001 wt%, the hydrates were able to grow films strong enough for testing in the standard 30-minute annealing time, allowing exploration of the effects of PVP on the interparticle force, film growth rate, sintering, and particle morphology. PVP reduced the baseline interparticle force by between 40 % and 54 %. PVP present in the water phase reduced film growth rates by between 34 % and 55%, while the particle concentration had little noticeable effect. The film growth retardation combined with the long-term shell strength/porosity effects led directly to a 20–40 % reduction in the magnitude of the force between sintered

particles and a 15–17 % slowing of sintering rate between 30 min and 1 h. The sintering results suggest that PVP adsorbed at the surface of the hydrate particles has anti-agglomerant like properties even at long contact times. This could be important in remediation or prevention of hydrate agglomerate formation, as the long-term effect of the PVP could allow more time to break up agglomerates.

Ultralow concentration PVP has a pronounced effect on particle scale morphology. The particles formed with PVP were typically rough and experienced large crater-like formations during initial growth and annealing. Particle morphologies also continued to change over time-scales ranging from 45 min to 2 h, indicating that the effects that PVP has on the hydrate particles are long lasting and can lead to noticeable shape changes. This has important implications in management of hydrate plug formation risk. A conceptual mechanism for the cause of the morphology changes was presented to aid in understanding how PVP altered the shapes of the hydrate particles. Areas of high PVP adsorption are hypothesized to have higher porosity and lower strength allowing diffusion of unconverted water out of the interior of the particle. This can cause a reduction in pressure within the particle, and the hydrate shell forms craters, which equalize the pressure. Understanding the effects of KHIs at very low concentrations would be important in reducing cost and environmental concern associated with KHI application. This is especially important when looking at KHIs as hydrate management strategies and determining how the effects of KHIs vary when employed below 1–3 wt%, such as in the case of injection failure or over dilution. The results of this work could be utilized to develop a screening tool for new KHIs and/or elucidate novel effects of existing KHIs at low concentrations.

Future work on the effect of subcooling on hydrate growth rates and morphology with a kinetic inhibitor would provide important information, though a different hydrate former may be considered to allow for a wider temperature range. Further, AFM or computational approaches could shed light on the changes in porosity caused by the addition of KHIs to hydrate forming systems, supporting this and other works on KHI effects.

CRediT authorship contribution statement

Josh Worley: Conceptualization, Methodology, Formal analysis, Investigation, Writing – original draft, review & editing. **Jose Delgado-Linares:** Conceptualization, Writing – original draft, review & editing. **Carolyn A. Koh:** Conceptualization, Writing – original draft, review & editing, Supervision.

Declaration of Competing Interest

The authors declare that they have no known competing financial interests or personal relationships that could have appeared to influence the work reported in this paper.

Data Availability

Data will be made available on request.

Acknowledgements

The authors thank the National Science Foundation, Award NSF-CBET 2015201 for funding. Thanks also to the Center for Hydrate Research for the facilities used for this study.

Appendix A. Supporting information

Supplementary data associated with this article can be found in the online version at doi:10.1016/j.colsurfa.2022.129825.

References

[1] E.D. Sloan, C.A. Koh. Clathrate hydrates of natural gases, third edition, CRC Press, 2007.
[2] Y.F. Makogon, Natural gas hydrates - a promising source of energy, J. Nat. Gas. Sci. Eng. 2 (2010), https://doi.org/10.1016/j.jngse.2009.12.004.
[3] J. Zheng, Z.R. Chong, M.F. Qureshi, P. Linga, Carbon dioxide sequestration via gas hydrates: a potential pathway toward decarbonization, Energy Fuels 34 (2020), https://doi.org/10.1021/acs.energyfuels.0c02309.
[4] A. Davoodabadi, A. Mahmoudi, H. Ghasemi, The potential of hydrogen hydrate as a future hydrogen storage medium, IScience 24 (2021), https://doi.org/10.1016/j.isci.2020.101907.
[5] H. Lee, J.W. Lee, D.Y. Kim, J. Park, Y.T. Seo, H. Zeng, I.L. Moudrakovskr, C. I. Ratcliffe, J.A. Ripmeester, Tuning clathrate hydrates for hydrogen storage, Nature 434 (2005), https://doi.org/10.1038/nature03457.
[6] N.I. Papadimitriou, I.N. Tsimpanogiannis, A.K. Stubos, Computational approach to study hydrogen storage in clathrate hydrates, Colloids Surf. A: Physicochem. Eng. Asp. 357 (2010), https://doi.org/10.1016/j.colsurfa.2009.10.003.
[7] E.D. Sloan, A changing hydrate paradigm - from apprehension to avoidance to risk management, Fluid Ph. Equilibria (2005), https://doi.org/10.1016/j.fluid.2004.08.009.
[8] C.A. Koh, E. Sloan, A. Sum, Natural Gas Hydrates in Flow Assurance, 2011. https://doi.org/10.1016/C2009–0-62311–4.
[9] A.K. Sum, C.A. Koh, E.D. Sloan, Clathrate hydrates: From laboratory science to engineering practice, Ind. Eng. Chem. Res. 48 (2009), https://doi.org/10.1021/ie900679m.
[10] S. Gao, Hydrate risk management at high watercuts with anti-agglomerant hydrate inhibitors, Energy Fuels 23 (2009), https://doi.org/10.1021/ef8009876.
[11] Z.M. Aman, Hydrate risk management in gas transmission lines, Energy Fuels 35 (2021), https://doi.org/10.1021/acs.energyfuels.1c01853.
[12] L.M. Frostman, V. Thieu, D.L. Crosby, H.H. Downs, Low-Dosage Hydrate Inhibitors (LDHIs): Reducing Costs in Existing Systems and Designing for the Future, in: 2003. https://doi.org/10.2118/80269-ms.
[13] D. Turner, Clathrate hydrate formation in water-in-oil dispersions, Ph.D. Thesis, Colorado School of Mines, 2005.
[14] H.M. Stoner, C.A. Koh, Perspective on the role of particle size measurements in gas hydrate agglomeration predictions, Fuel 304 (2021), https://doi.org/10.1016/j.fuel.2021.121385.
[15] M.A. Kelland, History of the development of low dosage hydrate inhibitors, Energy Fuels 20 (2006), https://doi.org/10.1021/ef050427x.
[16] B. Shi, S. Song, Y. Chen, X. Duan, Q. Liao, S. Fu, L. Liu, J. Sui, J. Jia, H. Liu, Y. Zhu, C. Song, D. Lin, T. Wang, J. Wang, H. Yao, J. Gong, Status of natural gas hydrate flow assurance research in china: a review, Energy Fuels 35 (2021), https://doi.org/10.1021/acs.energyfuels.0c04209.
[17] E.P. Brown, C.A. Koh, Competitive interfacial effects of surfactant chemicals on clathrate hydrate particle cohesion, Energy Fuels 30 (2016), https://doi.org/10.1021/acs.energyfuels.6b00145.
[18] M.A. Kelland, T.M. Svartås, L.D. Andersen, Gas hydrate anti-agglomerant properties of polypropoxylates and some other demulsifiers, J. Pet. Sci. Eng. 64 (2009), https://doi.org/10.1016/j.petrol.2008.12.001.
[19] M.A. Kelland, Production chemicals for the oil and gas industry, 2009. https://doi.org/10.1201/9781420092974.
[20] J. Yang, B. Tohidi, Characterization of inhibition mechanisms of kinetic hydrate inhibitors using ultrasonic test technique, Chem. Eng. Sci. 66 (2011), https://doi.org/10.1016/j.ces.2010.10.025.
[21] J.H. Sa, G.H. Kwak, K. Han, D. Ahn, K.H. Lee, Gas hydrate inhibition by perturbation of liquid water structure, Sci. Rep. 5 (2015), https://doi.org/10.1038/srep11526.
[22] E. Luna-Ortiz, M. Healey, R. Anderson, E. Sørhaug, Crystal growth inhibition studies for the qualification of a kinetic hydrate inhibitor under flowing and shut-in conditions, Energy Fuels 28 (2014), https://doi.org/10.1021/ef402493x.
[23] B.J. Anderson, J.W. Tester, G.P. Borghi, B.L. Trout, Properties of inhibitors of methane hydrate formation via molecular dynamics simulations, J. Am. Chem. Soc. 127 (2005), https://doi.org/10.1021/ja0554965.
[24] Y. Wang, S. Fan, X. Lang, Reviews of gas hydrate inhibitors in gas-dominant pipelines and application of kinetic hydrate inhibitors in China, Chin. J. Chem. Eng. 27 (2019), https://doi.org/10.1016/j.cjche.2019.02.023.
[25] R. Wu, Z.M. Aman, E.F. May, K.A. Kozielski, P.G. Hartley, N. Maeda, A.K. Sum, Effect of kinetic hydrate inhibitor polyvinylcaprolactam on cyclopentane hydrate cohesion forces and growth, Energy Fuels 28 (2014), https://doi.org/10.1021/ef500265w.
[26] Z.M. Aman, E.P. Brown, E.D. Sloan, A.K. Sum, C.A. Koh, Interfacial mechanisms governing cyclopentane clathrate hydrate adhesion/cohesion, Phys. Chem. Chem. Phys. 13 (2011), https://doi.org/10.1039/c1cp21907c.
[27] S. Dong, C. Liu, W. Han, M. Li, J. Zhang, G. Chen, The effect of the hydrate antiagglomerant on hydrate crystallization at the oil-water interface, ACS Omega 5 (2020), https://doi.org/10.1021/acsomega.9b03395.
[28] J. Chen, C.Y. Sun, B.Z. Peng, B. Liu, S. Si, M.L. Jia, L. Mu, K. le Yan, G.J. Chen, Screening and compounding of gas hydrate anti-agglomerants from commercial additives through morphology observation, Energy Fuels 27 (2013), https://doi.org/10.1021/ef400147j.
[29] E.P. Brown, D. Turner, G. Grasso, C.A. Koh, Effect of wax/anti-agglomerant interactions on hydrate depositing systems, Fuel 264 (2020), https://doi.org/10.1016/j.fuel.2019.116573.

[30] S.Y. Lee, H.C. Kim, J.D. Lee, Morphology study of methane-propane clathrate hydrates on the bubble surface in the presence of SDS or PVCap, J. Cryst. Growth 402 (2014), https://doi.org/10.1016/j.jcrysgro.2014.06.028.
[31] R. Larsen, C.A. Knight, E.D. Sloan, Clathrate hydrate growth and inhibition, Fluid Ph. Equilibria 150 (1998), https://doi.org/10.1016/s0378-3812(98)00335-5.
[32] M. Muraoka, M. Ohtake, Y. Yamamoto, Kinetic inhibition effect of type I and III antifreeze proteins on unidirectional tetrahydrofuran hydrate crystal growth, RSC Adv. 9 (2019), https://doi.org/10.1039/C9RA00627C.
[33] H. Sakaguchi, R. Ohmura, Y.H. Mori, Effects of kinetic inhibitors on the formation and growth of hydrate crystals at a liquid-liquid interface, J. Cryst. Growth 247 (2003), https://doi.org/10.1016/S0022-0248(02)02021-3.
[34] H. Bruusgaard, L.D. Lessard, P. Servio, Morphology study of structure i methane hydrate formation and decomposition of water droplets in the presence of biological and polymeric kinetic inhibitors, Cryst. Growth Des. 9 (2009), https://doi.org/10.1021/cg070568k.
[35] K. Dann, L. Rosenfeld, Surfactant effect on hydrate crystallization at the oil-water interface, Langmuir 34 (2018), https://doi.org/10.1021/acs.langmuir.8b00333.
[36] H. Hayama, M. Mitarai, H. Mori, J. Verrett, P. Servio, R. Ohmura, Surfactant effects on crystal growth dynamics and crystal morphology of methane hydrate formed at gas/liquid interface, Cryst. Growth Des. 16 (2016) 6084–6088, https://doi.org/10.1021/acs.cgd.6b01124.
[37] S. Yang, D.M. Kleehammer, Z. Huo, E.D. Sloan, K.T. Miller, Temperature dependence of particle–particle adherence forces in ice and clathrate hydrates, J. Colloid Interface Sci. 277 (2004) 335–341, https://doi.org/10.1016/j.jcis.2004.04.049.
[38] C.J. Taylor, L.E. Dieker, K.T. Miller, C.A. Koh, E.D. Sloan, Micromechanical adhesion force measurements between tetrahydrofuran hydrate particles, J. Colloid Interface Sci. 306 (2007) 255–261, https://doi.org/10.1016/j.jcis.2006.10.078.
[39] Zachary Aman, Interfacial Phenomena of Cyclopentane Hydrate, Ph.D. Thesis, Colorado School of Mines, 2012.
[40] C.A. Schneider, W.S. Rasband, K.W. Eliceiri, NIH Image to ImageJ: 25 years of image analysis, Nat. Methods 9 (2012), https://doi.org/10.1038/nmeth.2089.
[41] B.Z. Peng, A. Dandekar, C.Y. Sun, H. Luo, Q.L. Ma, W.X. Pang, G.J. Chen, Hydrate film growth on the surface of a gas bubble suspended in water, J. Phys. Chem. B 111 (2007) 12485–12493, https://doi.org/10.1021/jp074606m.
[42] Y.H. Mori, Estimating the thickness of hydrate films from their lateral growth rates: application of a simplified heat transfer model, J. Cryst. Growth 223 (2001) 206–212, https://doi.org/10.1016/S0022-0248(01)00614-5.
[43] V.A. Vlasov, Formation and dissociation of gas hydrate in terms of chemical kinetics, React. Kinet., Mech. Catal. 110 (2013) 5–13, https://doi.org/10.1007/s11144-013-0578-x.
[44] T. Mochizuki, Y.H. Mori, Simultaneous mass and heat transfer to/from the edge of a clathrate-hydrate film causing its growth along a water/guest-fluid phase boundary, Chem. Eng. Sci. 171 (2017) 61–75, https://doi.org/10.1016/j.ces.2017.05.015.
[45] C.J. Taylor, K.T. Miller, C.A. Koh, E.D. Sloan, Macroscopic investigation of hydrate film growth at the hydrocarbon/water interface, Chem. Eng. Sci. 62 (2007) 6524–6533, https://doi.org/10.1016/j.ces.2007.07.038.
[46] H.D. Nagashima, M. Oshima, Y. Jin, Film-growth rates of methane hydrate on ice surfaces, J. Cryst. Growth 537 (2020), 125595, https://doi.org/10.1016/j.jcrysgro.2020.125595.
[47] S. Almenningen, M. Lysyy, G. Ersland, Quantification of CH_4 hydrate film growth rates in micromodel pores, Cryst. Growth Des. 21 (2021) 4090–4099, https://doi.org/10.1021/acs.cgd.1c00396.
[48] H.M. Stoner, A. Phan, A. Striolo, C.A. Koh, Water wettability coupled with film growth on realistic cyclopentane hydrate surfaces, Langmuir 37 (2021) 12447–12456, https://doi.org/10.1021/acs.langmuir.1c02136.
[49] L.U. Udegbunam, J.R. DuQuesnay, L. Osorio, V.K. Walker, J.G. Beltran, Phase equilibria, kinetics and morphology of methane hydrate inhibited by antifreeze proteins: application of a novel 3-in-1 method, J. Chem. Thermodyn. 117 (2018), https://doi.org/10.1016/j.jct.2017.08.015.
[50] R. Wu, K.A. Kozielski, P.G. Hartley, E.F. May, J. Boxall, N. Maeda, Methane-propane mixed gas hydrate film growth on the surface of water and Luvicap EG solutions, Energy Fuels 27 (2013), https://doi.org/10.1021/ef4003268.
[51] Y.F. Makogon, T.Y. Makogon, S.A. Holditch, Kinetics and mechanisms of gas hydrate formation and dissociation with inhibitors, in: N.Y. Ann (Ed.), Acad. Sci. (2000), https://doi.org/10.1111/j.1749-6632.2000.tb06833.x.
[52] B.D. Fleming, E.J. Wanless, Soft-contact atomic force microscopy imaging of adsorbed surfactant and polymer layers, Microsc. Microanal. 6 (2000), https://doi.org/10.1007/s100059910009.
[53] R. Gordienko, H. Ohno, V.K. Singh, Z. Jia, J.A. Ripmeester, V.K. Walker, Towards a green hydrate inhibitor: Imaging antifreeze proteins on clathrates, PLoS ONE 5 (2010), https://doi.org/10.1371/journal.pone.0008953.
[54] S. Perez Huertas, K. Terpilowski, M. Wisniewska, V. Zarko, Influence of polyvinylpyrrolidone adsorption on stability of silica aqueous suspension - effects of polymer concentration and solid content, Physicochem. Probl. Miner. Process. 53 (2017), https://doi.org/10.5277/ppmp170110.
[55] J. Jiang, Y. Shen, D. Yu, T. Yang, M. Wu, L. Yang, M. Petru, Porous film coating enabled by polyvinyl pyrrolidone (Pvp) for enhanced air permeability of fabrics: the effect of pvp molecule weight and dosage, Polymers 12 (2020), https://doi.org/10.3390/polym12122961.